

# Scattering on a rectangular potential barrier in nodal-line Weyl semimetals

D.A. Khokhlov,<sup>1,2</sup> A.L. Rakhmanov,<sup>1,2,3</sup> and A.V. Rozhkov<sup>1,3</sup>

<sup>1</sup>*Moscow Institute for Physics and Technology (State University), Moscow region, 141700 Russia*

<sup>2</sup>*Dukhov Research Institute of Automatics, Moscow, 127055 Russia*

<sup>3</sup>*Institute for Theoretical and Applied Electrodynamics,  
Russian Academy of Sciences, Moscow, 125412 Russia*

(Dated: September 19, 2018)

We investigate single-particle ballistic scattering on a rectangular barrier in the nodal-line Weyl semimetals. Since the system under study has a crystallographic anisotropy, the scattering properties are dependent on mutual orientation of the crystalline axis and the barrier. To account for the anisotropy, we examine two different barrier orientations. It is demonstrated that, for certain angles of incidence, the incoming particle passes through the barrier with probability of unity. This is a manifestation of the Klein tunneling, a familiar phenomenon in the context of graphene and semimetals with Weyl points. However, the Klein tunneling in the Weyl-ring systems is observed when the angle of incidence differs from  $90^\circ$ , unlike the cases of graphene and Weyl-point semimetals. The reflectionless transmission also occurs for the so-called ‘magic angles’. The values of ‘the magic angles’ are determined by geometrical resonances between the barrier width and the de Broglie length of the scattered particle. In addition, we show that under certain conditions the wave function of the transmitted and reflected particles may be a superposition of two plane waves with unequal momenta. Such a feature is a consequence of the non-trivial structure of the iso-energy surfaces of the nodal-line semimetals.

PACS numbers:

## I. INTRODUCTION

Topological semimetals (TSMs) were predicted theoretically<sup>1-7</sup> and then discovered experimentally<sup>8-11</sup>. The main feature of the TSMs is that the valence and conduction bands intersect in several (nodal) points or closed (nodal) lines in momentum space<sup>2,5,12</sup>. Thus, in contrast to a usual metal with a two-dimensional Fermi surface, the Fermi surface of a three-dimensional TSM is reduced to a finite set of points or curves. Specifically, for the nodal-line semimetals, which we discuss below, the Fermi surface is shrunk to a curve.

Within a simplest theoretical framework<sup>4</sup>, the nodal line (or ring) of a Weyl semimetal is a closed plane curve in a three-dimensional Brillouin zone<sup>2-4,13</sup>. In the plane of the nodal line, which we will also refer to as the basal plane, the kinetic energies of the electrons and holes are proportional to the square of the distance from the nodal line. As the momentum deviates from the nodal line in the direction normal to the basal plane, the energy variation is proportional to this deviation.

Since the spectrum of the nodal-ring semimetals is rather peculiar, one can expect some unusual scattering effects in these materials. For example, the electron and hole bands touch each other near the Fermi energy in the TSMs, and even weak spatial variation of the potential energy can lead to the interband transitions. Consequently, a single-particle scattering problem must take into account both electron and hole states. This is a necessary condition for observation of the Klein phenomenon, that is, a process in which a particle passes through high and long potential barrier without reflection<sup>14,15</sup>. Klein tunneling was described theoretically<sup>15,16</sup> and observed experimentally<sup>17</sup> in graphene. It suppresses

the backscattering, thus contributing to the increase of the graphene electron mean free path. It is known that the Klein phenomenon requires linear single-particle spectrum. Since electron dispersion in the nodal-ring semimetals is linear in some directions in  $\mathbf{k}$ -space, the Klein tunneling might be expected in these materials under certain conditions.

Here we study the scattering of an electron by a step-wise potential barrier in the ballistic regime. Four different cases are considered: barriers with finite and infinite width, both perpendicular and parallel to the basal plane. We demonstrate that reflectionless tunneling is possible for both orientations of the barrier. Similar to the graphene<sup>15</sup>, the perfect transmission in the nodal-ring semimetals is associated with both Klein tunneling and ‘magic angles’ resonances<sup>18</sup>. The Klein phenomenon in the nodal-ring semimetals is observed if the incident angle of the particle differs from  $90^\circ$ . This is dissimilar to the case of graphene and Weyl-point semimetals, where this effect exists only for normal incidence.

Another interesting feature of the scattering in the studied materials is the emergence of two transmission and two reflection channels for a single incident plane wave. To characterize such a scattering one needs two transmission and two reflection coefficients. The transmitted (reflected) particles in different transmission (reflection) channels have different momenta. This property is in stark contrast with the scattering of free non-relativistic electrons, where the momentum of the outgoing particles are uniquely fixed by the momentum of the incident particle. The existence of the multiple scattering channels is a consequence of the complicated dispersion structure of a nodal-ring semimetal.

The paper is organized as follows. In Sec. II we briefly

discuss the theoretical model of a nodal-ring semimetal. This model is used in Sec. III to study the scattering on a barrier parallel to the basal plane. The barrier perpendicular to the basal plane is discussed in Sec. IV. Summary and conclusions are in Sec. V.

## II. MODEL

We write the Hamiltonian of the system in the following form<sup>4</sup>:

$$\hat{H}(\mathbf{k}) = (m - Bk_{\perp}^2)\sigma_x + k_z\sigma_z + U\sigma_0, \quad (1)$$

where  $\mathbf{k} = (k_x, k_y, k_z)$  is the single-particle momentum, and scalar  $k_{\perp}$  is determined by the formula  $k_{\perp}^2 = k_x^2 + k_y^2$ , coefficient  $m$  is an analog of the rest mass, the quantity  $1/(2B)$  is an inertial mass for the motion in the  $xy$ -plane, and  $U$  is the potential energy. Matrix  $\sigma_0$  is the 2x2 unity matrix and  $\sigma_{x,z}$  are the Pauli matrices. We set  $\hbar$  and  $v_F$  in  $z$  direction equal to one. The spectrum of Hamiltonian (1) is

$$\varepsilon_{\mathbf{k}}^{e,h} = U \pm \sqrt{(m - Bk_{\perp}^2)^2 + k_z^2}, \quad (2)$$

where label ‘e’ (‘h’) corresponds to electrons (holes). If the potential energy is zero, the solutions of the equation  $\varepsilon_{\mathbf{k}} = 0$  forms a circle of radius  $k_{\perp} = \sqrt{m/B}$  in the  $xy$ -plane. This circle is the nodal line of the model, and  $xy$ -plane is the basal plane. Normalized eigenfunctions of the Hamiltonian (1) are spinors

$$\psi_{\mathbf{k}} = C_{\mathbf{k}} \begin{pmatrix} 1 \\ \chi_{\mathbf{k}} \end{pmatrix}, \quad \chi_{\mathbf{k}} = \frac{\varepsilon - U - k_z}{m - Bk_{\perp}^2}, \quad C_{\mathbf{k}} = \frac{1}{\sqrt{1 + \chi_{\mathbf{k}}^2}}. \quad (3)$$

Following a standard procedure<sup>19</sup>, we can calculate the probability current associated with a plane wave  $\psi(\mathbf{r}) = a\psi_{\mathbf{k}}e^{i\mathbf{k}\mathbf{r}}$ :

$$\mathbf{j} = |a|^2 \begin{pmatrix} -4\chi_{\mathbf{k}}Bk_x \\ -4\chi_{\mathbf{k}}Bk_y \\ 1 - \chi_{\mathbf{k}}^2 \end{pmatrix}. \quad (4)$$

This current is invariant with respect to rotation in the  $xy$ -plane. We will use Eq. (4) below to choose a correct structure of the outgoing waves and to define properly transmission and reflection coefficients.

## III. BARRIER PARALLEL TO BASAL PLANE

First we consider the situation when the barrier is parallel to the basal plane, see Fig. 1. The potential energy  $U(z) = U[\theta(z) - \theta(z - L)]$ , where  $\theta(z)$  is the Heaviside step-function, depends on  $z$  coordinate only. Barrier width in the  $z$  direction is equal to  $L$ . In the  $x$  and  $y$  directions the barrier extends to infinity. Thus, the momentum components  $k_x$  and  $k_y$  are conserved. Further,

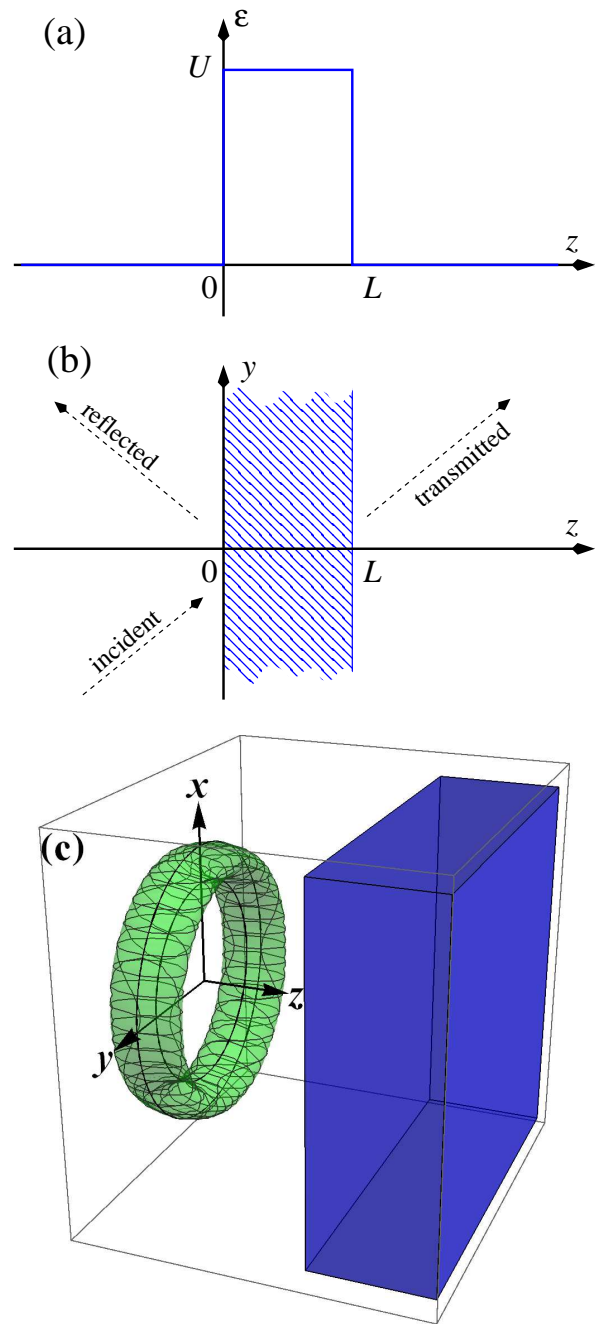


FIG. 1: Barrier parallel to the basal plane. Panel (a): Potential energy  $U(z)$ . It is finite and constant for  $0 < z < L$ . Otherwise, it is zero. Panel (b): Incident, reflected, and transmitted waves near the barrier. The wave vectors of the incoming and outgoing waves are shown schematically by the dashed lines with arrows. The barrier is represented by the blue hatched area. Panel (c): Relative orientations of the barrier and the iso-energy surface. The iso-energy surface is defined by the equation  $\varepsilon^2 = (m - Bk_{\perp}^2)^2 + k_z^2$ . It is shown by (green) torus in the reciprocal space. The barrier is shown as blue parallelepiped.

we assume that the incident particle is an electron (not a hole). The barrier divides the space into three regions (to the left of the barrier, to the right of the barrier, and under it). The wave function in these three regions is

$$\begin{aligned}\psi &= C_+ e^{ik_z z} \begin{pmatrix} 1 \\ \chi_+ \end{pmatrix} + r C_- e^{-ik_z z} \begin{pmatrix} 1 \\ \chi_- \end{pmatrix}, \quad z < 0, \\ \psi &= D e^{iq_z z} \begin{pmatrix} 1 \\ \phi_+ \end{pmatrix} + F e^{-iq_z z} \begin{pmatrix} 1 \\ \phi_- \end{pmatrix}, \quad 0 < z < L, \\ \psi &= t C_+ e^{ik_z(z-L)} \begin{pmatrix} 1 \\ \chi_+ \end{pmatrix}, \quad z > L.\end{aligned}\quad (5)$$

Here

$$k_z = \sqrt{\varepsilon^2 - (m - Bk_\perp^2)^2}, \quad (6)$$

$$q_z = \sqrt{(\varepsilon - U)^2 - (m - Bk_\perp^2)^2}. \quad (7)$$

The quantities  $\pm k_z$  and  $\pm q_z$  are the  $z$ -components of the wave vectors outside and inside the barrier, respectively. Energy of the incident electron is  $\varepsilon$ , and

$$\chi_\pm = \chi(\pm k_z) = \frac{\varepsilon \mp k_z}{m - Bk_\perp^2}, \quad (8)$$

$$\phi_\pm = \phi(\pm q_z) = \frac{\varepsilon - U \mp q_z}{m - Bk_\perp^2},$$

$$C_\pm = (1 + \chi_\pm^2)^{-1/2}.$$

Factor  $e^{ik_x x + ik_y y}$ , common for all three wave functions, is omitted for brevity. To describe a particle propagating freely outside the barrier, the wave function must have purely real  $k_z$ , or, equivalently,

$$\frac{m - \varepsilon}{B} < k_\perp^2 < \frac{m + \varepsilon}{B}. \quad (9)$$

Transmission and reflection coefficients  $T = |t|^2$  and  $R = |r|^2$  obey the usual relation  $T + R = 1$ . To derive  $r$  and  $t$  we should match  $\psi$  at  $z = 0$  and  $z = L$ , accounting for the continuity of the probability current. In this way we derive

$$\begin{aligned}C_+ \begin{pmatrix} 1 \\ \chi_+ \end{pmatrix} + r C_- \begin{pmatrix} 1 \\ \chi_- \end{pmatrix} &= D \begin{pmatrix} 1 \\ \phi_+ \end{pmatrix} + F \begin{pmatrix} 1 \\ \phi_- \end{pmatrix}, \\ t C_+ \begin{pmatrix} 1 \\ \chi_+ \end{pmatrix} &= D e^{iq_z L} \begin{pmatrix} 1 \\ \phi_+ \end{pmatrix} + F e^{-iq_z L} \begin{pmatrix} 1 \\ \phi_- \end{pmatrix}.\end{aligned}\quad (10)$$

Solving system (10) one obtains the expression for  $r$

$$r = \frac{(U - k_z)^2 - q_z^2}{k_z^2 + q_z^2 - U^2 + 2ik_z q_z \cot(q_z L)} \sqrt{\frac{\varepsilon + k_z}{\varepsilon - k_z}}. \quad (11)$$

The dependence of the transmission coefficient  $T = 1 - |r|^2$  on the transverse momentum  $k_\perp$  is calculated using Eq. (11). The results for several energies  $\varepsilon$  are shown in Fig. 2. The same dependence for different barrier widths  $L$  is presented in Fig. 3. We see that for certain parameter values the transmission is perfect:  $T = 1$ ,

or, equivalently,  $r = 0$ . Note that  $k_\perp$  varies in the interval defined by the conditions (9).

As it follows from Eqs. (2), (6), (7), and (11), the disappearance of the reflected wave ( $r = 0$ ) occurs when either of two different conditions is satisfied. The first one is

$$q_z L = \pi n, \quad (12)$$

where  $n$  is an integer. It includes the barrier width  $L$  and corresponds to a dimensional phenomenon similar to the Ramsauer-Townsend effect<sup>20</sup>. Unlike the classical Ramsauer-Townsend effect, which occurs for a non-relativistic quantum particle, whose energy exceeds the barrier height, for Weyl semimetals, below-the-barrier particles may also demonstrate the same reflectionless transmission. Similar phenomenon has been observed in graphene: electrons approaching a rectangular barrier at the so-called ‘magic angles’ propagate through the barrier without reflection<sup>18</sup>. The Ramsauer-Townsend-like peaks in  $T(k_\perp)$  become more pronounced with the increase of  $L$ , see Fig. 3.

If relation (12) is violated, coefficient  $r$  still can vanish, provided that

$$k_\perp = \sqrt{m/B}. \quad (13)$$

Under this condition  $\varepsilon = k_z = U - q_z$ , the Hamiltonian (1) effectively describes a one-dimensional relativistic particle, and the Klein scattering is observed. Thus, while both Eqs. (12) and (13) correspond to the reflectionless transmission of the incident particle, the mechanisms responsible for such a transmission are non-identical.

If  $q_z$  is real, the wave function under the barrier is described by a linear combination of plane waves. From Eq. (7) we derive that  $\text{Im } q_z = 0$  when

$$\frac{m - |\varepsilon - U|}{B} < k_\perp^2 < \frac{m + |\varepsilon - U|}{B}. \quad (14)$$

If this condition is violated, parameter  $q_z$  becomes imaginary, and probability for the electron to pass through the barrier vanishes exponentially with the growth of  $L$ . As a result, the value of  $T$  rapidly decays outside the range of  $k_\perp$  defined by Eq. (14). The curve at  $\varepsilon/m = 0.9$  in Fig. 2 illustrates this feature.

In the above discussion we assumed the ballistic regime of the electron scattering. Such an approach is valid if the electron mean-free path  $l_{\text{mf}}$  is larger than the barrier width. For a wider barrier,  $l_{\text{mf}} \ll L$ , the electron scattering on the barrier edge at  $z = L$  becomes insignificant, which is equivalent to the limit  $L \rightarrow \infty$ , the case of a  $p$ - $n$  junction. Thus, we have no reflected wave within the barrier and have to match wave function at  $z = 0$  only. Solving the system of two linear equations we obtain the expression for the reflected wave amplitude in the form

$$r = \sqrt{\frac{\varepsilon + k_z}{\varepsilon - k_z}} \frac{k_z - U - q_z}{k_z + U + q_z}. \quad (15)$$

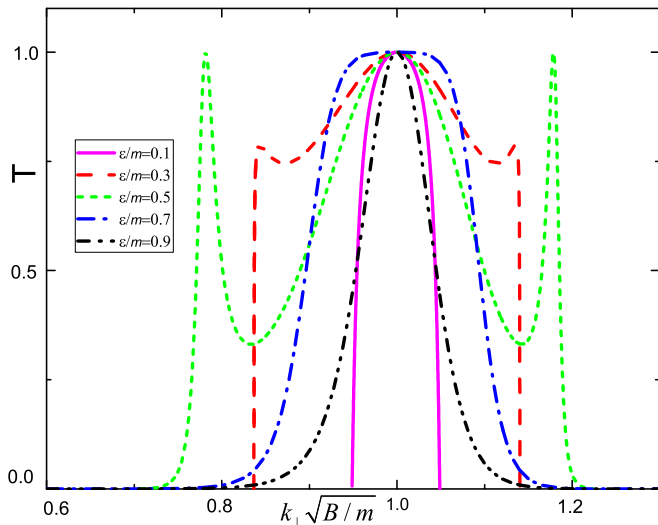


FIG. 2: Transmission coefficient  $T$  as a function of the dimensionless transverse momentum  $k_{\perp} \sqrt{B/m}$  for different values of the ratio  $\varepsilon/m$  (see legend in the figure). The curves are calculated for  $U/m = 1$ ,  $mL = 10$ , and  $Bm = 1$ . Momentum  $k_{\perp}$  is limited by the conditions  $\sqrt{(m-\varepsilon)/B} < k_{\perp} < \sqrt{(m+\varepsilon)/B}$ , which guarantees that a propagating solution ( $\text{Im} k_z = 0$ ) exists. When  $k_{\perp} \sqrt{B/m} = 1$ , a perfect transmission due to the Klein tunneling is observed. In addition, the reflectionless tunneling at the so-called ‘magic angles’ is also possible.

In the limit  $k_{\perp} \rightarrow \sqrt{m/B}$ , when  $k_z \rightarrow \varepsilon$ , we obtain

$$r \propto \sqrt{\varepsilon - k_z}. \quad (16)$$

Thus, the reflection coefficient vanishes and the Klein tunneling is observed. Naturally, no ‘magic angles’ exist in the case of the infinite barrier.

#### IV. BARRIER PERPENDICULAR TO BASAL PLANE

Let us consider the situation when the rectangular barrier is perpendicular to the basal plane. Such a configuration is depicted in Fig. 4. The nodal ring lies in the  $xy$ -plane, as before. We fix  $y$ -axis to be normal to the barrier. In such a geometry momentum components  $k_x$  and  $k_z$  are preserved by the scattering process. As for  $k_y$ , we derive from Eq. (2) that  $k_y = \pm k_y^{(\pm)}$ , where

$$k_y^{(\pm)} = \sqrt{\frac{1}{B} \left( m - Bk_x^2 \pm \sqrt{\varepsilon^2 - k_z^2} \right)}. \quad (17)$$

We see that four different values of  $k_y$  correspond to a single set of parameters  $(k_x, k_z, \varepsilon)$ . Therefore, an incident electron can be scattered by the barrier into four possible channels  $k_y = \pm k_y^{(\pm)}$ , see Fig. 4. In other words, the flux of incident electrons is distributed between two transmission channels and two reflection channels. To distinguish

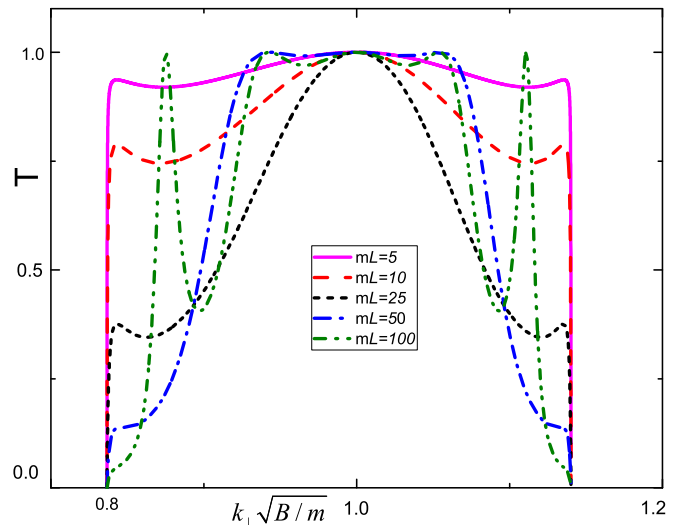


FIG. 3: Transmission coefficient  $T$  as a function of the dimensionless momentum  $k_{\perp} \sqrt{B/m}$  for different dimensionless barrier widths  $mL$  (see legend in the figure). The curves are calculated for  $U/m = 1$ ,  $\varepsilon/m = 0.3$ , and  $Bm = 1$ . When  $k_{\perp} \sqrt{B/m} = 1$ , perfect transmission due to the Klein tunneling is observed. In addition, the reflectionless tunneling at the so-called ‘magic angles’ is also possible. The latter becomes more pronounced for wider barriers.

between the transmission and reflection channels we can use Eq. (4) to make sure that the transmitted particle carries positive current  $j_y$  along  $y$ -axis. One can easily check that  $k_y = k_y^{(+)}$  and  $k_y = -k_y^{(-)}$  correspond to the transmission channels,  $j_y > 0$ , while  $k_y = -k_y^{(+)}$  and  $k_y = k_y^{(-)}$  correspond to the reflection channel,  $j_y < 0$ . If  $m - Bk_x^2 \geq \sqrt{\varepsilon^2 - k_z^2}$  the scattering into four channels is possible. Otherwise, the value of  $k_y^{(-)}$  is imaginary, and the transmission and reflection channels corresponding to  $k_y^{(-)}$  disappear.

Under the barrier, the wave function is also a linear combination of four exponentials, each characterized by a specific value of  $q_y$ . Possible values of  $q_y$  are  $\pm q_y^{(\pm)}$ , where

$$q_y^{(\pm)} = \sqrt{\frac{1}{B} \left[ m - Bk_x^2 \pm \sqrt{(\varepsilon - U)^2 - k_z^2} \right]}. \quad (18)$$

We will confine the following discussion by two constraints. First, we will assume that the incoming electron is characterized by the momentum projection  $k_y = k_y^{(+)}$ . The incoming electron with  $k_y = -k_y^{(-)}$  will not be studied. Second, only the limit  $k_x = 0$  will be explicitly discussed. Non-zero  $k_x$  may be easily accounted for by the renormalization of parameter  $m$ . With this in mind, we can write the wave function to the left of the barrier ( $y < 0$ ) as a sum of the incident plane wave and two reflected plane waves:

$$\psi_1 = e^{ik_y^{(+)}y} \begin{pmatrix} 1 \\ -\chi \end{pmatrix} + r_+ e^{-ik_y^{(+)}y} \begin{pmatrix} 1 \\ -\chi \end{pmatrix} + r_- e^{ik_y^{(-)}y} \begin{pmatrix} 1 \\ \chi \end{pmatrix}, \quad (19)$$

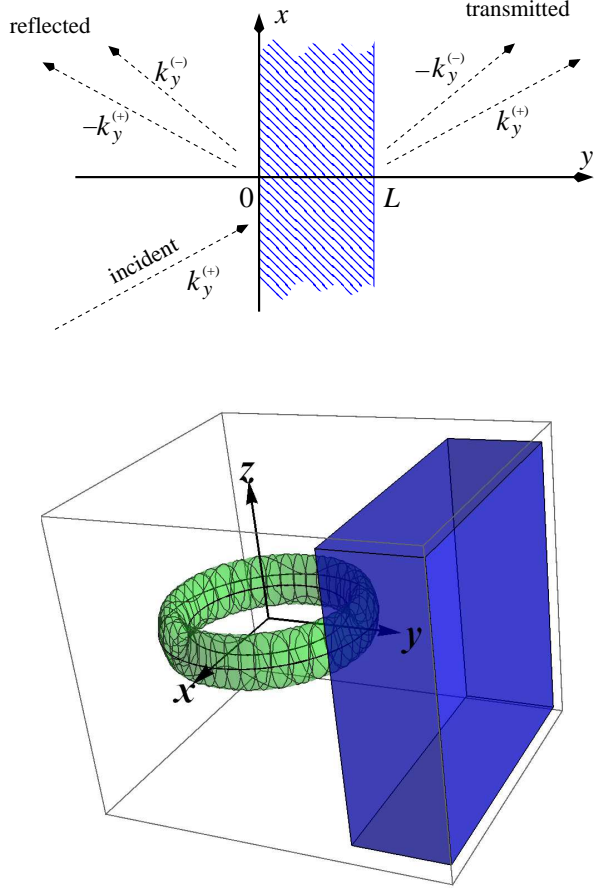


FIG. 4: Barrier perpendicular to the basal plane. Top panel: Incident, reflected, and transmitted waves near the barrier. The wave vectors of the incoming and outgoing waves are shown by the dashed lines with arrows. The barrier is represented by the blue hatched area. The barrier has finite width equal to  $L$  in the  $y$  direction and extends to infinity in the  $x$  and  $z$  directions. Bottom panel: Relative orientation of the barrier and the iso-energy surface. The iso-energy (green) surface, defined by the equation  $\varepsilon^2 = (m - Bk_{\perp}^2)^2 + k_z^2$ , is a torus in the reciprocal space. The barrier is shown as blue rectangular parallelepiped. Within the parallelepiped the potential energy is  $U$ , outside it is zero.

where

$$\chi = \sqrt{\frac{\varepsilon - k_z}{\varepsilon + k_z}}. \quad (20)$$

In the region under the barrier ( $0 < y < L$ ), the wave function can be expressed as

$$\begin{aligned} \psi_2 = & \tilde{a}_- e^{iq_y^{(-)}y} \begin{pmatrix} 1 \\ \phi \end{pmatrix} + \tilde{b}_- e^{-iq_y^{(-)}y} \begin{pmatrix} 1 \\ \phi \end{pmatrix} \\ & + \tilde{a}_+ e^{iq_y^{(+)}y} \begin{pmatrix} 1 \\ -\phi \end{pmatrix} + \tilde{b}_+ e^{-iq_y^{(+)}y} \begin{pmatrix} 1 \\ -\phi \end{pmatrix}, \end{aligned} \quad (21)$$

where

$$\phi = \sqrt{\frac{\varepsilon - U - k_z}{\varepsilon - U + k_z}}. \quad (22)$$

Finally, to the right of the barrier ( $y > L$ ), we have

$$\psi_3 = t_- e^{-ik_y^{(-)}(y-L)} \begin{pmatrix} 1 \\ \chi \end{pmatrix} + t_+ e^{ik_y^{(+)}(y-L)} \begin{pmatrix} 1 \\ -\chi \end{pmatrix}. \quad (23)$$

The continuity of the probability current at the barrier edges requires the continuity of the wave function and its  $y$ -derivative at  $y = 0$  and  $y = L$ . As a result, we obtain

$$\begin{aligned} (1+r_+) \begin{pmatrix} 1 \\ -\chi \end{pmatrix} + r_- \begin{pmatrix} 1 \\ \chi \end{pmatrix} &= (\tilde{a}_- + \tilde{b}_-) \begin{pmatrix} 1 \\ \phi \end{pmatrix} + (\tilde{a}_+ + \tilde{b}_+) \begin{pmatrix} 1 \\ -\phi \end{pmatrix}, \\ k_y^{(+)}(1-r_+) \begin{pmatrix} 1 \\ -\chi \end{pmatrix} + r_- k_y^{(-)} \begin{pmatrix} 1 \\ \chi \end{pmatrix} &= q_y^{(-)}(\tilde{a}_- - \tilde{b}_-) \begin{pmatrix} 1 \\ \phi \end{pmatrix} \\ &+ q_y^{(+)}(\tilde{a}_+ - \tilde{b}_+) \begin{pmatrix} 1 \\ -\phi \end{pmatrix}, \\ (\tilde{a}_- e^{iq_y^{(-)}L} + \tilde{b}_- e^{-iq_y^{(-)}L}) \begin{pmatrix} 1 \\ \phi \end{pmatrix} &+ (\tilde{a}_+ e^{iq_y^{(+)}L} + \tilde{b}_+ e^{-iq_y^{(+)}L}) \begin{pmatrix} 1 \\ -\phi \end{pmatrix} \\ = t_- \begin{pmatrix} 1 \\ \chi \end{pmatrix} + t_+ \begin{pmatrix} 1 \\ -\chi \end{pmatrix}, \\ q_y^{(-)}(\tilde{a}_- e^{iq_y^{(-)}L} - \tilde{b}_- e^{-iq_y^{(-)}L}) \begin{pmatrix} 1 \\ \phi \end{pmatrix} &+ \\ q_y^{(+)}(\tilde{a}_+ e^{iq_y^{(+)}L} - \tilde{b}_+ e^{-iq_y^{(+)}L}) \begin{pmatrix} 1 \\ -\phi \end{pmatrix} &= k_y^{(-)} t_- \begin{pmatrix} 1 \\ \chi \end{pmatrix} + k_y^{(+)} t_+ \begin{pmatrix} 1 \\ -\chi \end{pmatrix}. \end{aligned} \quad (24)$$

Solving these equations numerically, we calculate the amplitudes  $r_{\pm}$ ,  $t_{\pm}$ , and obtain two transmission coefficients  $T_{\pm} = |t_{\pm}|^2$  and two reflection coefficients  $R_{\pm} = |r_{\pm}|^2$ . Particle conservation implies that  $T_+ + T_- + R_+ + R_- = 1$ . The results of the calculations are shown in Figs. 5 and 6, where transmission and reflection coefficients are plotted as functions of  $\varepsilon$  for different parameter values.

When the energy  $\varepsilon$  is within the interval  $k_z < \varepsilon < \sqrt{k_z^2 + m^2}$ , the quantities  $k_y^{(\pm)}$  are all real. Consequently, all four scattering channels are open. Under this conditions the scattering of the incident wave with  $k_y^{(+)}$  to the reflected wave with  $k_y^{(-)}$  may be significant. It becomes particularly strong if  $\varepsilon$  is close to  $k_z$ : in this regime  $R_- \rightarrow 1$  when  $\varepsilon \rightarrow k_z$ , see Fig. 5. At the opposite end of the considered energy interval,  $\varepsilon \rightarrow \sqrt{k_z^2 + m^2}$ , the reflection probabilities vanish, and the incident particle passes through the barrier without reflection, preserving its momentum.

An analytical expressions for the transmission and reflection coefficients can be obtained in the limit  $k_z = 0$ , when the incident particle momentum lies in  $xy$ -plane. (Since  $k_z$  is conserved, the momenta of the transmitted and reflected particles are confined to the basal plane as well.) In such a situation Hamiltonian (1) decouples into two copies of a scalar non-relativistic Hamiltonian with the spectrum  $\varepsilon(k_y, k_z = 0) = \pm(m - Bk_y^2)$ , and  $\chi = \phi = 1$ . It is easy to check that a particle with the momentum component  $k_y^{(+)} = \sqrt{(m + \varepsilon)/B}$  cannot

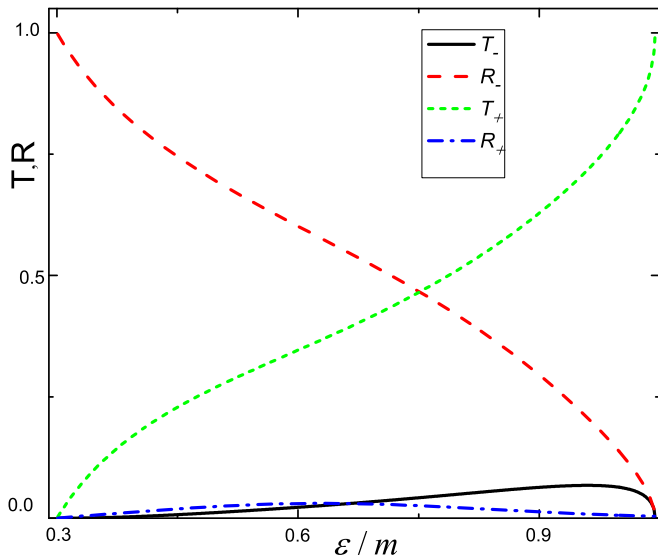


FIG. 5: Transmission and reflection coefficients as functions of energy. The curves are calculated for  $k_z/m = 0.3$ ,  $U/m = 1$ ,  $mL = 5$  and  $Bm = 1$ . Coefficients  $T_{\pm}(R_{\pm})$  correspond to the transmitted (reflected) waves with  $k_y^{(\pm)}$ . We assume that  $k_x = 0$  because nonzero  $k_x$  only renormalizes  $m$ .

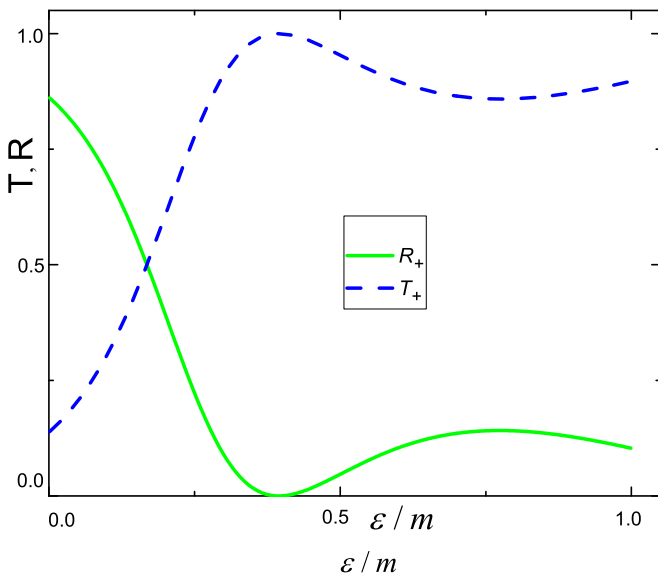


FIG. 6: Transmission and reflection coefficients versus energy for the scattering confined to the basal plane ( $k_z = 0$ ). The curves are calculated for  $U/m = 1$ ,  $mL = 5$  and  $B = 1/m$ . Coefficients  $T_{\pm}(R_{\pm})$  describe the transmitted (reflected) waves with  $k_y^{(\pm)}$ . In this regime both  $T_-$  and  $R_-$  vanish. We assume that  $k_x = 0$  because nonzero  $k_x$  only renormalizes  $m$ .

be scattered to  $k_y^{(-)}$  channel since  $k_y^{(+)}$  and  $k_y^{(-)}$  belong to different sectors. Solving Eqs. (24) in this limit, we obtain  $R_- = T_- = 0$  and

$$R_+ = \frac{[(q_y^{(-)})^2 - (k_y^{(+)})^2] \sin^2(q_y^{(-)}L)}{4(q_y^{(-)}k_y^{(+)})^2 + [(q_y^{(-)})^2 - (k_y^{(+)})^2] \sin^2(q_y^{(-)}L)}, \quad (25)$$

where  $q_y^{(-)} = \sqrt{(m - |\varepsilon - U|)/B}$ . The dependencies of  $R_+$  and  $T_+ = 1 - R_+$  versus  $\varepsilon$  are shown in Fig. 6. These functions are non-monotone due to dimensional oscillating factor  $\sin^2(q_y^{(-)}L)$ . Equation (25) is, in some respects, similar to the expression describing scattering of a non-relativistic particle on a rectangular barrier<sup>21</sup>. However, there is an important difference. The transmission coefficient of a non-relativistic particle  $T_{\text{nrrel}}(\varepsilon)$  oscillates due to dimensional effect if  $\varepsilon > U$ , but is monotone if  $\varepsilon < U$ . In the case of the nodal-ring semimetal, the functions  $R_+(\varepsilon)$  and, consequently,  $T_+(\varepsilon)$  are non-monotone even for  $\varepsilon < U$ . Mathematically, this occurs due to the existence of the plane wave solutions with  $\text{Im } q_y^{(-)} = 0$  in the regime  $\varepsilon < U$ .

The case of the infinite-length barrier can be considered in the same manner. After matching the wave function and its derivative at the barrier edge, reflection coefficients  $R_{\pm}$  can be calculated. In general, both of them are non-zero, that is, the scattering in four channels is possible. In the limit  $k_z = 0$  we can find explicit formulas

$$R_+ = \left( \frac{k_y^{(+)} - q_y^{(+)}}{k_y^{(+)} + q_y^{(+)}} \right)^2, \quad T_+ = \left( \frac{2k_y^{(+)}}{k_y^{(+)} + q_y^{(+)}} \right)^2, \quad (26)$$

$$R_- = T_- = 0.$$

This result is similar to the case of the scattering of non-relativistic particle.

## V. CONCLUSION

We show that the electron scattering in the nodal-line semimetals demonstrates unusual features, such as the Klein tunneling, reflectionless transmission at ‘magic angles’ (which is an analogue of the classical Ramsauer-Townsend effect), and the emergence of the additional scattering channels.

The Klein tunneling occurs for a barrier parallel to the basal plane. The momentum of the incident particle must satisfy the condition  $m - Bk_{\perp}^2 = 0$ . If these requirements are met, Hamiltonian (1) effectively describes one-dimensional massless fermions, for which the Klein tunneling is a well-established phenomenon.

Besides the Klein tunneling, reflectionless propagation across the barrier can be observed for a particle colliding with the barrier at certain ‘magic angles’. These angles depend on the barrier width. Such a behavior is related to the Ramsauer-Townsend effect for a non-relativistic quantum particle. Similar phenomena discussed for graphene<sup>18</sup>. However, the classical Ramsauer-Townsend effect exists for a particle whose energy exceeds the height of the barrier, while in the nodal-line semimetals a particle with  $\varepsilon < U$  also demonstrates the same reflectionless propagation.

When the barrier is perpendicular to the basal plane, the Klein tunneling is impossible. In this configuration another interesting phenomenon can be observed:

the second scattering channel becomes available both for transmitted and reflected particles. Such an unusual scattering occurs because the system of equations describing conservation of the electron energy and momentum has two different roots. Therefore, two different values of  $|k_y|$  are admissible. The first of these values is the same as  $|k_y|$  of the incident particle, while the second differs. Thus, the wave functions of the transmitted and reflected particles are superpositions of two states with unequal momenta. Depending on the scattering parameters, the probability of changing  $|k_y|$  after a scattering

event can be substantial. We prove this for scattering processes confined to the basal plane.

### Acknowledgments

This work was supported by the Presidium of RAS (Program I.7, Modern problems of photonics, the probing of inhomogeneous media and materials).

- 
- <sup>1</sup> A. A. Burkov, "Topological semimetals," *Nat. Mater.* **15**, 1145 (2016).
  - <sup>2</sup> A. A. Burkov, M. D. Hook, and L. Balents, "Topological nodal semimetals," *Phys. Rev. B* **84**, 235126 (2011).
  - <sup>3</sup> C. Fang, Y. Chen, H.-Y. Kee, and L. Fu, "Topological nodal line semimetals with and without spin-orbital coupling," *Phys. Rev. B* **92**, 081201 (2015).
  - <sup>4</sup> Z. Yan, P.-W. Huang, and Z. Wang, "Collective modes in nodal line semimetals," *Phys. Rev. B* **93**, 085138 (2016).
  - <sup>5</sup> A. A. Burkov and L. Balents, "Weyl Semimetal in a Topological Insulator Multilayer," *Phys. Rev. Lett.* **107**, 127205 (2011).
  - <sup>6</sup> Y. Kim, B. J. Wieder, C. L. Kane, and A. M. Rappe, "Dirac Line Nodes in Inversion-Symmetric Crystals," *Phys. Rev. Lett.* **115**, 036806 (2015).
  - <sup>7</sup> H. Weng, C. Fang, Z. Fang, B. A. Bernevig, and X. Dai, "Weyl Semimetal Phase in Noncentrosymmetric Transition-Metal Monophosphides," *Phys. Rev. X* **5**, 011029 (2015).
  - <sup>8</sup> M. Neupane, S.-Y. Xu, R. Sankar, N. Alidoust, G. Bian, C. Liu, I. Belopolski, T.-R. Chang, H.-T. Jeng, H. Lin, et al., "Observation of a three-dimensional topological Dirac semimetal phase in high-mobility  $\text{Cd}_3\text{As}_2$ ," *Nat. Commun.* **5** (2014).
  - <sup>9</sup> L. S. Xie, L. M. Schoop, E. M. Seibel, Q. D. Gibson, W. Xie, and R. J. Cava, "A new form of  $\text{Ca}_3\text{P}_2$  with a ring of Dirac nodes," *APL Materials* **3**, 083602 (2015).
  - <sup>10</sup> M. Neupane, I. Belopolski, M. M. Hosen, D. S. Sanchez, R. Sankar, M. Szlawska, S.-Y. Xu, K. Dimitri, N. Dhakal, P. Maldonado, et al., "Observation of topological nodal fermion semimetal phase in  $\text{ZrSiS}$ ," *Phys. Rev. B* **93**, 201104 (2016).
  - <sup>11</sup> R. Yu, H. Weng, Z. Fang, X. Dai, and X. Hu, "Topological Node-Line Semimetal and Dirac Semimetal State in Antiperovskite  $\text{Cu}_3\text{PdN}$ ," *Phys. Rev. Lett.* **115**, 036807 (2015).
  - <sup>12</sup> X. Wan, A. M. Turner, A. Vishwanath, and S. Y. Savrasov, "Topological semimetal and Fermi-arc surface states in the electronic structure of pyrochlore iridates," *Phys. Rev. B* **83**, 205101 (2011).
  - <sup>13</sup> C. Fang, H. Weng, X. Dai, and Z. Fang, "Topological nodal line semimetals," *Chin. Phys. B* **25**, 117106 (2016).
  - <sup>14</sup> O. Klein, "Die Reflexion von Elektronen an einem Potentialsprung nach der relativistischen Dynamik von Dirac," *Zeitschrift für Physik A Hadrons and Nuclei* **53**, 157 (1929).
  - <sup>15</sup> M. I. Katsnelson, K. S. Novoselov, and A. K. Geim, "Chiral tunnelling and the Klein paradox in graphene," *Nat. Phys.* **2**, 620 (2006).
  - <sup>16</sup> A. Rozhkov, A. Sboychakov, A. Rakhmanov, and F. Nori, "Electronic properties of graphene-based bilayer systems," *Phys. Rep.* **648**, 1 (2016).
  - <sup>17</sup> A. F. Young and P. Kim, "Quantum interference and Klein tunnelling in graphene heterojunctions," *Nat. Phys.* **5**, 222 (2009).
  - <sup>18</sup> T. Tudorovskiy, K. J. A. Reijnders, and M. I. Katsnelson, "Chiral tunneling in single-layer and bilayer graphene," *Phys. Scripta* **2012**, 014010 (2012).
  - <sup>19</sup> L. Landau and E. Lifshitz, *Quantum Mechanics, Non-Relativistic Theory: Vol. 3 of Course of Theoretical Physics* (1981).
  - <sup>20</sup> C. Ramsauer, "Über den Wirkungsquerschnitt der Gasmoleküle gegenüber langsamen Elektronen," *Annalen* **369**, 513 (1921).
  - <sup>21</sup> D. J. Griffiths, *Introduction to Quantum Mechanics* (Cambridge University Press, 2016).